

Integrated *ab initio* modelling of atomic order and magnetic anisotropy for rare-earth-free magnet design: effects of alloying additions in L1₀ FeNi

Christopher D. Woodgate,^{1,*} Laura H. Lewis,^{2,3} and Julie B. Staunton^{1,†}

¹*Department of Physics, University of Warwick, Coventry, CV4 7AL, United Kingdom*

²*Department of Chemical Engineering, Northeastern University, Boston, MA 02115, USA*

³*Department of Mechanical and Industrial Engineering,
Northeastern University, Boston, MA 02115, USA*

(Dated: January 5, 2024)

We describe an integrated modelling approach to accelerate the search for novel, single-phase, multicomponent materials with high magnetocrystalline anisotropy (MCA). For a given system we predict the nature of atomic ordering, its dependence on the magnetic state, and then proceed to describe the consequent MCA. Crucially, within our modelling framework, the same *ab initio* description of the material's electronic structure determines both aspects. We demonstrate this holistic method by studying the effects of alloying additions in FeNi, examining systems with the general stoichiometry Fe₄Ni₃X, including X = Pt, Pd, Al, and Co. The atomic ordering behaviour predicted on adding these elements, fundamental for determining a material's MCA, is rich and varied. Equiatomic FeNi has been reported to require ferromagnetic order to establish the tetragonal L1₀ order suited for significant MCA. Our results show that when alloying additions are included in this material, annealing in an applied magnetic field and/or below a material's Curie temperature may also promote tetragonal order, along with an appreciable effect on the predicted MCA.

I. INTRODUCTION

Permanent magnets play a crucial role in modern society, with applications in electrical power generation and conversion, essential in the global transition to clean energy. The 'gold-standard' of current permanent magnetic materials are those based on the rare-earth elements, such as Nd₂Fe₁₄B [1, 2] and SmCo₅ [3], which have large magnetic energy products and are widely used in applications [4]. However, the rare-earth elements are a constrained resource, with issues around the stability of the supply chain, price volatility, and the environmental impact of their extraction [5–7]. There is therefore a desire to develop new materials which use reduced concentrations of rare-earth elements, or no rare-earth elements at all. In addition, there is currently a 'gap' in permanent magnet performance between the rare-earth-based supermagnets and the significantly weaker oxide ferrite magnets [8].

Computational modelling approaches have an important role to play in the process of materials discovery. Not only can they be used to screen potential compositions to suggest which are stable and have the desired physical properties for a particular application, but via an *ab initio* description of materials' electronic structure, they also have the potential to advance fundamental physical understanding of why existing materials perform the way they do. This insight can facilitate the optimisation of materials for applications, as well as guide the search for improved compositions and processing techniques.

In this work, we demonstrate a new computational

technique which enables holistic assessment of a magnetic alloy's phase behaviour and subsequent magnetocrystalline anisotropy, and is therefore suitable for the discovery of new magnetic materials. As a case study, we apply the approach to suggest new alloy compositions for use as advanced permanent magnets. We begin by describing in detail the binary FeNi system, which is currently under consideration as a potential 'gap' magnet [9]. We then proceed to consider the addition of a third alloying element, studying systems with the composition Fe₄Ni₃X. The approach is based on complementary techniques for studying the phase behaviour of multicomponent alloys [10–13] and the magnetocrystalline anisotropy of (partially) ordered intermetallic phases [14–16]. Crucially, both the phase behaviour of a material and its magnetocrystalline anisotropy are examined on the same first-principles footing, enabling us to examine how the electronic 'glue' of an alloy drives atomic ordering and produces subsequent magnetic properties. This holistic approach is important; it will always be possible to computationally design metastable structures with extraordinary magnetic properties, but for any proposed material to be useful, it must be able to be synthesised in the laboratory.

Our workflow for holistically studying the phase stability and subsequent magnetic properties of a given alloy composition, illustrated in Fig. 1, proceeds as follows. First, using the Korringa-Kohn-Rostoker (KKR) [17] formulation of density functional theory (DFT) [18], we generate the self-consistent potentials and associated electron density of the disordered alloy—the solid solution—where averaging over substitutional atomic disorder is performed using the coherent potential approximation (CPA) [19]. Then, using the $S^{(2)}$ theory for multicomponent alloys [10–13], we perform a linear response analysis to rigorously calculate the two-point correlation function,

* Christopher.Woodgate@warwick.ac.uk

† J.B.Staunton@warwick.ac.uk

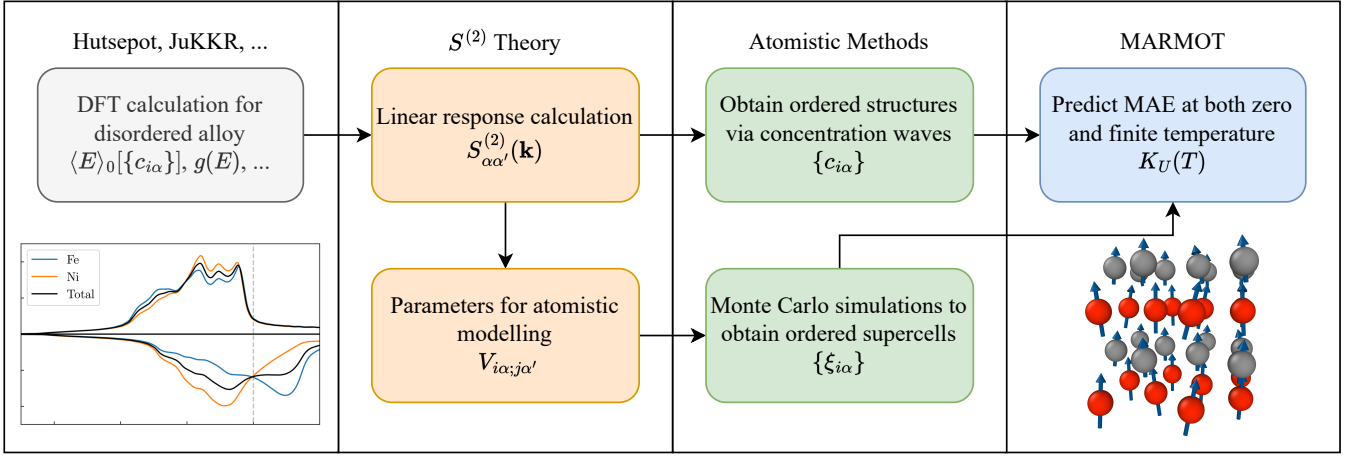


FIG. 1. Visualisation of the workflow used in this paper for holistically assessing the phase behaviour and subsequent magnetic properties of a given alloy composition.

an atomic short-range order (ASRO) parameter, *ab initio*. From this linear-response calculation, we can infer (partial) chemical orderings directly using a concentration wave analysis [20], or instead fit to a pairwise Hamiltonian describing the internal energy of the alloy that is suitable for atomistic modelling. Once the (partially) ordered phase of interest has been established, we are able to use a DFT-based description of the magnetic torque at both zero and finite temperature to assess the system's magnetocrystalline anisotropy [14, 16].

A. Recipe for a Good Permanent Magnet

Before presenting the case study of ordered FeNi, it is worth discussing the desirable intrinsic physical properties a material must possess to be suitable for advanced permanent magnetic applications. Putting aside the consideration of shape anisotropy, used to produce magnets such as those of the Alnico family [21], there are three intrinsic physical quantities which determine a material's suitability for use as an advanced permanent magnet. First is the Curie temperature, T_C , the temperature below which spontaneous magnetisation occurs even in the absence of an applied magnetic field [22]. Second is the saturation magnetisation, \mathbf{M}_S , which is the material's magnetic polarization when fully magnetised [23]. Third is its magnetocrystalline anisotropy (MCA), which measures the energetic cost of rotating the magnetisation vector, \mathbf{M} , away from the material's energetically favorable 'easy axis' established at the atomic level by spin-orbit coupling and crystal symmetry considerations [24]. The MCA can be related to a material's coercivity, an extrinsic, structure-sensitive property that is a measure of the energetic cost of demagnetising the material [25]. In turn, the coercivity leads to a figure of merit known as the 'maximum energy product' which can be used to quantitatively compare the performance different permanent

magnets at a given temperature [25].

Ideally, a permanent magnet will have a high Curie temperature, well above its desired operating temperature, to ensure that its magnetisation remains large during operation. Inevitably, this means that 3d transition metals must be incorporated, such as Fe or Co which have high elemental Curie temperatures of 1043 and 1388 K respectively [26]. While it is the highly localised *f* electrons of elements such as Nd and Sm which give rise to the extraordinary magnetic energy products of the rare-earth supermagnets [27], all use significant quantities of Fe or Co in their compositions. This is because these transition metals often stabilise magnetic order at high temperatures and can therefore play a crucial role in determining materials' hard magnetic properties during operation [28]. Similarly, a good permanent magnet will have a large saturation magnetisation, which again requires the use of 3d elements such as Fe and Co in any candidate composition.

The MCA of a material is determined by a material's crystal structure and the associated local crystallographic environment around magnetic moments. Permanent magnets generally possess a uniaxial crystal structure [25], typically tetragonal or hexagonal. These uniaxial crystal structures give rise to uniaxial magnetocrystalline anisotropy, K , to leading order, of the form [24]

$$K = K_1 \sin^2 \theta \quad (1)$$

where θ describes the angle of rotation of the magnetisation away from the easy crystal axis, and K_1 is the magnetocrystalline anisotropy constant. In conjunction with a large saturation magnetisation, \mathbf{M}_S , a value of K_1 larger than approximately 1 MJm^{-3} , is considered to be necessary for a material to be of use as a permanent magnet for advanced applications [8].

In summary, in the search for novel permanent magnets for applications it is necessary to search for a stable intermetallic compound with a uniaxial crystal structure

(and associated uniaxial magnetocrystalline anisotropy), a high Curie temperature, and high saturation magnetisation. In addition, with regard to the aforementioned economic and environmental considerations, compositions should be pursued that use reduced concentrations of constrained elements such as Nd, Sm, and Co, as well as noble metals.

B. $L1_0$ Materials

A class of materials which fulfill all of the above requirements are those intermetallic compounds forming on the face-centred cubic (fcc) lattice and crystallising in the $L1_0$ structure, visualised in Fig. 2. This family includes materials already experimentally verified to have superb magnetic properties, such as FePt [14, 29], FePd [16, 30], and CoPt [31, 32], but also includes materials consisting entirely of comparatively cheap, abundant elements such as MnAl [33, 34] and FeNi [9, 35, 36]. In the present work, as a demonstration of our modelling approach, we will focus on the last of these materials, $L1_0$ FeNi.

Although $L1_0$ FeNi (the meteoritic mineral tetrataenite) does not have a theoretically predicted maximum energy product as large as those of the rare-earth supermagnets [9], the relative abundance and availability of its constituent elements, in conjunction with its anticipated production based on principles used in steel processing, mean that its environmental footprint could be significantly lower than for rare-earth-based magnets. In addition,

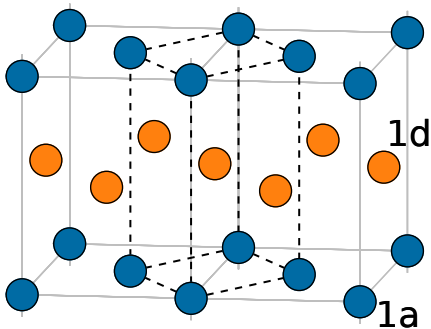


FIG. 2. Visualisation of $L1_0$ ordered structure imposed on the face-centred cubic lattice. The conventional simple tetragonal (st) cell is indicated by dashed black lines and contains two non-equivalent sites with Wyckoff labels 1a and 1d. The 1a sites are at the corners of the cell, while the 1d site is at the centre. This st unit cell has lattice parameters $c' = a$, $a' = b' = a/\sqrt{2}$, where a is the conventional fcc lattice parameter. The simple tetragonal representation, with its minimal two-atom basis and a cell elongated in the \hat{z} direction than in makes the origin of a uniaxial anisotropy in $L1_0$ materials clear.

while there remain many open questions concerning tetrataenite's predicted maximum energy product, it is projected to be higher than those of weak magnetic materials such as Alnico and the oxide ferrite magnets [9, 36]. As such, tetrataenite may be poised to fill the current gap in permanent magnetic performance and accessibility.

However, $L1_0$ FeNi proves to be extremely challenging to synthesise in a laboratory setting. Although the $L1_0$ phase is reported to be stable at typical operating temperatures for applications [37], its formation is restricted by a low atomic ordering temperature and consequently sluggish kinetics [35, 38]. As a result, the fcc solid solution (Strukturbericht designation A1) is retained to room temperature, only ordering very slowly under conventional processing techniques. Typically, bulk samples observed experimentally either come from meteorites [39], which have cooled slowly over a period of millions of years; have had their atomic mobility improved during the annealing process *e.g.* by bombardment with high-energy neutrons [35, 38]; or have had their structure modified to foster faster diffusion, *e.g.* through severe plastic deformation [40].

II. RESULTS

A. FeNi

We begin our case study by examining the phase behaviour and magnetocrystalline anisotropy of the equiatomic binary system, FeNi. Using the all-electron HUTSEPOT code [41], we perform self-consistent calculations within the KKR-CPA formulation of DFT [17] to model the electronic structure of the disordered fcc (A1) phase in both its paramagnetic and ferromagnetic states.

Fig. 3 shows the total and species-resolved density of states for the A1 phase in both its paramagnetic and ferromagnetic states, where the paramagnetic phase is modelling within the disordered local moment (DLM) picture [42–44]. The broken magnetic symmetry in the ferromagnetic state can most clearly be seen to differentiate the bonding contributions from majority and minority spin electrons, owing to the different exchange splitting of d -states associated with Fe and Ni. This response is expected to significantly alter both the nature of predicted atomic ordering in the system, and the temperature at which this ordering emerges.

We then use our linear response theory to assess the phase behaviour of this system in both its paramagnetic and ferromagnetic states. The $S^{(2)}$ theory for multicomponent alloys [10] has previously been used with success to study atomic arrangements in the Cantor alloy (CrMnFeCoNi) and its derivatives [11], the refractory high-entropy alloys [12], and to examine the impact of magnetic ordering on atomic arrangements [13]. The theory works with partial atomic occupancies of lattice sites, $\{c_{i\alpha}\}$. For example, for the binary FeNi solid solution, for each site i in the underlying fcc lattice, $c_{i\alpha} = 0.5$

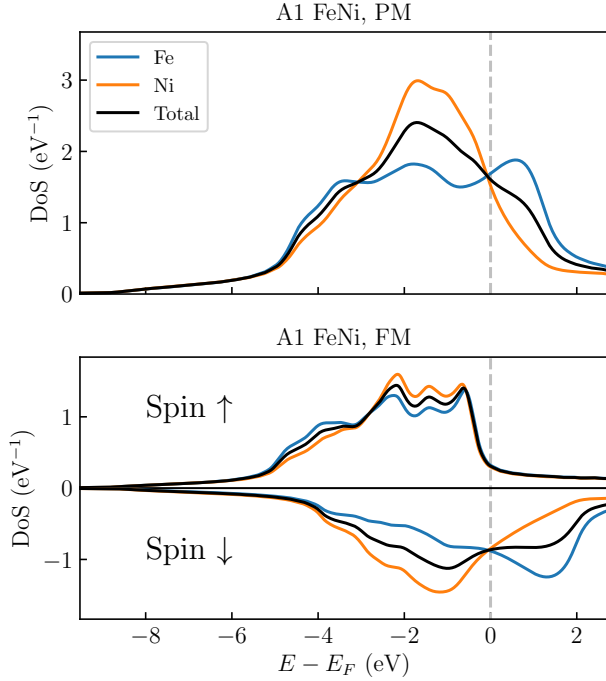


FIG. 3. Species-resolved density of states for disordered (A1) FeNi in its paramagnetic (left) and ferromagnetic (right) states. The paramagnetic state is modelled within the disordered local moment picture. The total DoS curve is given by the average of the species-resolved curves, weighted by their concentrations. For the ferromagnetic state, the upper half of the plot represents the majority-spin DoS, while the bottom half represents the DoS in the minority spin channel. Magnetic order can be seen to clearly alter the nature of the contributions to the total DoS from both Fe and Ni, owing to the significant difference in exchange splitting of Fe and Ni d -states.

for both $\alpha = 1$ (Fe) and $\alpha = 2$ (Ni). The theory then uses the language of concentration waves [20] to describe ordered structures, writing

$$c_{i\alpha} = c_\alpha + \sum_{\mathbf{k}} e^{i\mathbf{k} \cdot \mathbf{R}_i} \Delta c_\alpha(\mathbf{k}). \quad (2)$$

The overall (average) concentration is represented by c_α , while an applied chemical fluctuation (concentration wave) is denoted $\Delta c_\alpha(\mathbf{k})$. For example, the L1₀ structure is specified by $\mathbf{k} = (0, 0, 1)$, in units of $\frac{2\pi}{a}$, and $\Delta c_{1(2)} = +(-)0.5$ describing alternating layers of Fe and Ni atoms. (For clarity, when tabulating results, we choose to normalise the chemical fluctuation, writing $\Delta\alpha = \Delta c_\alpha / \|\Delta c_\alpha\|$, as this allows the relative size of fluctuations to be objectively compared.) The analysis of the alloy's phase stability then proceeds by performing a Landau-type series expansion of the free energy of the system, allowing the energetic cost of various imposed chemical fluctuations to be assessed. This Landau-type theory allows us to infer the highest temperature T_{ord} at which, for some \mathbf{k}_{ord} , there is a chemical

fluctuation Δc_α that renders the solid solution unstable, resulting in a chemical ordering. Crucially, the chemical polarisation [11], Δc_α , informs us how the chemical species partition themselves onto the various sublattices of the predicted ordered structure. The $S^{(2)}$ theory is fully first-principled, and leads to a linear response calculation based on the self-consistent one-electron potentials generated using HUTSEPOT to infer chemical ordering. These potentials can be non-magnetic [12], ferromagnetic [13], or paramagnetic [11], as appropriate to the system considered.

Predicted ordering temperatures, wavevectors, and chemical polarisations for FeNi are tabulated in I. Notably, L1₀ ordering, characterised by the wavevector $\mathbf{k}_{\text{ord}} = (0, 0, 1)$, is only predicted when we model the material when it is in its ferromagnetic state, reflective of the electronic structure of the material below its Curie temperature. The predicted ordering temperature is 507 K, which compares reasonably well with other theoretical [45] estimates and experimental [35] determinations. These results are highly significant; they suggest that any materials processing aiming to synthesise the L1₀ form of FeNi must be carried out below its Curie temperature. It may also be possible that heat treatment of the sample in an applied magnetic field will promote chemical ordering, as applying a magnetic field could induce a (small) spin polarisation to the system [13].

In addition to the above linear response analysis of the phase stability, the $S^{(2)}$ theory also enables extraction of lattice-based atom-atom interaction energies for further atomistic modelling of the phase behaviour of a system. This approach is based on discrete site occupancies, $\{\xi_{i\alpha}\}$, where $\xi_{i\alpha}=1$ if site i is occupied by an atom of species α , and $\xi_{i\alpha}=0$ otherwise. The internal energy of the system is described by the conventional Bragg-Williams Hamiltonian [46, 47], which takes the form

$$H(\{\xi_{i\alpha}\}) = \frac{1}{2} \sum_{i\alpha; j\alpha'} V_{i\alpha; j\alpha'} \xi_{i\alpha} \xi_{j\alpha'}. \quad (3)$$

The phase behaviour of the system can then be simulated

Magnetic State	T_{ord} (K)	\mathbf{k}_{ord}	Δ Fe	Δ Ni
Paramagnetic	175	(0, 0.675, 0.675)	0.707	-0.707
Ferromagnetic	507	(0, 0, 1)	0.707	-0.707

TABLE I. Comparison of the predicted atomic ordering temperatures and concentration wave modes for FeNi in both its paramagnetic and ferromagnetic states. Note that we choose to normalise the chemical fluctuation, writing $\Delta\alpha = \Delta c_\alpha / \|\Delta c_\alpha\|$. The paramagnetic state is modelled within the disordered local moment picture. It is only when the ferromagnetic state is modelled that an L1₀ ordering (indicated by $\mathbf{k}_{\text{ord}} = (0, 0, 1)$) is predicted. This suggests that any materials processing aiming to achieve L1₀ atomic ordering needs to be performed when the material is below its Curie temperature.

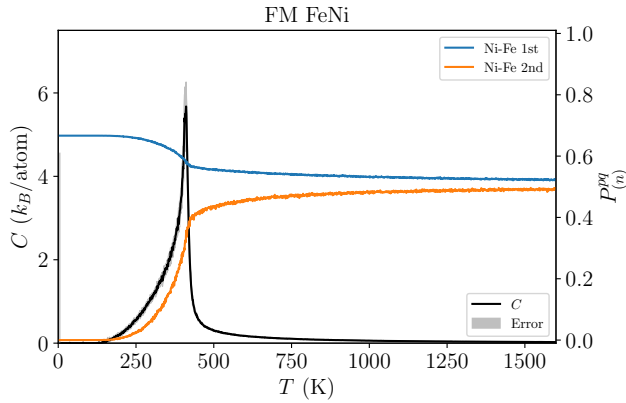


FIG. 4. Atomic order parameters (P_n^{pq}) and specific heat capacity (C) as a function of temperature from lattice-based Monte Carlo simulations for the FeNi system modelled in its ferromagnetic (FM) state. The phase transition just below 500 K is a transition from the atomically disordered fcc (A1) phase to the atomically ordered L1₀ phase.

using sampling methods such as the Metropolis Monte Carlo algorithm [48].

For FeNi, our computed atom-atom interaction energies are tabulated in the Supplemental Material [66]. Using these interactions, we perform simulated annealing on an ensemble of 10 simulations of systems of 2048 atoms with periodic boundary conditions applied, and using atomic-swaps rather than substitutions to conserve the overall concentration of each species [48]. To assess the nature of atomic ordering in the system, we use conditional probabilities averaged over configurations, denoted P_n^{pq} , representing the probability of species p being an n^{th} nearest-neighbour of species q . These parameters therefore represent atomic short-range order (ASRO) parameters. Using the fluctuation-dissipation theorem, it is also possible to estimate the specific heat capacity of the simulated system [48], which helps to identify the temperature at which phase transitions occur.

Visualised in Fig. 4 are our ASRO parameters and specific heat capacity determinations as a function of temperature for FeNi in its ferromagnetic state. The A1-L1₀ phase transition is characterised by $P_1^{\text{Fe-Ni}} = 1/3$, and $P_2^{\text{Fe-Ni}} = 0$, which occurs a little below 500 K in our simulations, consistent with the result obtained from the linear response analysis, and confirms the L1₀ structure as the ground-state of the system.

Given a predicted atomically ordered structure, such as L1₀ FeNi, we use the same first-principles-based framework to describe its magnetic characteristics and, therefore, suitability for applications. Within our framework, we generate new HUTSEPOT [41] potentials for the predicted (partially) ordered phases, and then use the MARMOT [49] code to calculate the phases' magnetic properties at both zero and finite temperature [14]. Our $S^{(2)}$ theory is based on the same underlying formulation of DFT as is used in MARMOT, and therefore we have an

integrated description of the electrons driving both chemical ordering and producing the magnetic properties.

We calculate the MCA for perfect L1₀ FeNi at zero-temperature using the same lattice parameters as was employed for the linear response calculation ($c/a = 1$) to be $K_1 = 0.94 \text{ MJm}^{-3}$. Experimental estimates [35, 38, 39, 50–57] have put the MCA of this material in the region $0.2\text{--}0.93 \text{ MJm}^{-3}$, while previous theoretical calculations [36, 37, 58–65] have obtained values in the range $0.34\text{--}0.96 \text{ MJm}^{-3}$. Our magnetisation of $M = 1.66 \mu_B/\text{atom}$ is also consistent with earlier theoretical [11, 64, 65] and experimental [56] studies. We therefore take these results as verification that our treatment models the L1₀ FeNi system successfully.

B. Fe₄Ni₃Pt

To promote atomic ordering and enhance magnetocrystalline anisotropy in this class of materials, one approach to consider is the addition of a third alloying element [67]. As an illustrative example of the effects of such alloying additions on atomic arrangements in this material, we consider the addition of a small amount of Pt to the (Fe,Ni) solid solution. Although Pt is unlikely to ever find its way into a mass-produced magnet on account of its high cost and low abundance, it is known that the binary FePt system readily crystallises into the L1₀-structure with an atomic ordering temperature of around 1600 K [68]. In addition, the L1₀ phase of FePt is known to have a large MCA energy ($K_1 \simeq 15 \text{ MJm}^{-3}$) attributed to the heavy $5d$ Pt atoms driving large spin-orbit coupling [14]. Our expectation is that the addition of Pt to FeNi to form Fe(Ni,Pt) could yield an energetically stable intermetallic phase with magnetocrystalline anisotropy between that of FeNi and FePt. As a demonstration, we consider the substitution of Pt at a concentration of 12.5%, *i.e.* studying a system with the overall composition Fe₄Ni₃Pt.

First, in a naive calculation, we calculate the magnetocrystalline anisotropy of this system assuming that Pt exclusively occupies sites on the Ni sublattice in the L1₀ structure. That is, the 1a site is occupied by pure Fe, while the 1d site has chemical occupancy Ni_{0.75}Pt_{0.25}. Under this assumption, a MCA of $K_1 = 3.44 \text{ MJm}^{-3}$ is computed, a value significantly larger than that for obtained pure L1₀ FeNi. However, this calculation does not account for the phase stability of the compound. To assess the likelihood of formation of the ordered phase, we again apply the $S^{(2)}$ theory for multicomponent alloys [10–13] to this composition.

Tabulated in II are predicted atomic ordering temperatures, concentration wavevectors, and chemical polarisations for Fe₄Ni₃Pt in both its paramagnetic and ferromagnetic states. In contrast to results obtained for pure FeNi, the wavevector associated with ordering of the Pt-modified composition is found to be $\mathbf{k}_{\text{ord}} = (0, 0, 1)$ in both magnetic states. The predicted atomic order-

ing temperatures are likewise similar, initially suggesting that the magnetic state of the disordered phase might not be as critical to the onset of atomic ordering in the Pt-modified material as in the binary FeNi. However, when the chemical polarisation of the concentration wave is inspected, it can be seen that both the paramagnetic and ferromagnetic orderings are characterised by the arrangements of the Pt atoms, with Fe and Ni distributions largely unaffected and remaining disordered. We associate this dominance with the relative atomic size difference between the 3d elements Fe and Ni, and the larger 5d element Pt, an effect which has been noted in alloys such as the Ni-Pt system.

From this linear response calculation, we infer an L1₀ ordering in both ferromagnetic and paramagnetic states, and at higher temperatures than for the FeNi binary. To predict the (partial) atomic site occupancies, we take the chemical polarisation of the concentration wave and allow this concentration wave to ‘grow’ until (at least) one chemical species has an associated lattice site occupancy of zero, this being the most atomically ordered structure consistent with the concentration wave. For the atomic ordering predicted for the paramagnetic solid solution, the 1a site occupancy is given by Fe_{0.614}Ni_{0.386}, while the 1d site occupancy is given by Fe_{0.386}Ni_{0.364}Pt_{0.25}. (See Fig. 2 for reference.) The computed MCA for this ordered state when the alloy is quenched to low temperatures is $K_1 = 0.96 \text{ MJm}^{-3}$, a value that is only fractionally larger than that of pure FeNi. However, for the solid solution in a ferromagnetic state, the predicted atomic ordering better separates Fe and Ni, with the 1a site occupancy for this condition as Fe_{0.678}Ni_{0.322} and the 1d site occupancy as Fe_{0.322}Ni_{0.428}Pt_{0.25}. The computed MCA is now higher, at $K_1 = 1.22 \text{ MJm}^{-3}$, a value that is *larger* than the predicted MCA for maximally ordered, unmodified L1₀ FeNi.

In a multicomponent alloy system such as the Fe₄Ni₃Pt composition, the linear response calculation may not convey a full picture of the nature of atomic order in the system. However, we are able to recover a simple pairwise atomistic model from it and perform further Monte Carlo simulations to better understand the nature of the atomic arrangements. (See Fig. 1 for an overview of the work-

Magnetic State	T_{ord} (K)	\mathbf{k}_{ord}	$\Delta \text{ Fe}$	$\Delta \text{ Ni}$	$\Delta \text{ Pt}$
Paramagnetic	794	(0, 0, 1)	0.672	0.065	-0.737
Ferromagnetic	1163	(0, 0, 1)	0.795	-0.237	-0.558

TABLE II. Comparison of the predicted atomic ordering temperatures and concentration wave modes for Fe₄Ni₃Pt in both its paramagnetic and ferromagnetic states. The paramagnetic state is modelled within the disordered local moment picture. Both orderings are dominated by Pt, on account of the relative atomic size difference between it and the smaller 3d elements Fe and Ni, however there is better distinguishment between Fe and Ni in the ferromagnetic state.

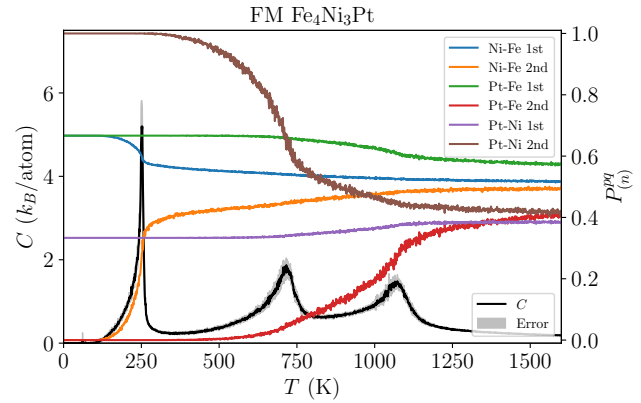


FIG. 5. Atomic order parameters (P_n^{pq}) and specific heat capacity (C) as a function of temperature from lattice-based Monte Carlo simulations for the Fe₄Ni₃Pt system modelled in its ferromagnetic (FM) state. There are three predicted phase transitions, indicated by the three peaks in the specific heat capacity, with the tetragonal Fe-Ni ordering occurring at the lowest temperature.

flow.) Visualised in Fig. 5 are atomic radial distribution probabilities and a measure of the configurational contribution to the specific heat capacity (SHC) of the system. It can be seen that there are in fact three distinct crystallographic orderings which can occur. The first ordering, at relatively high temperature, is cubic and Pt-driven—it represents Pt occupying the corners of the parent fcc lattice, with Ni and Fe arranged in a disordered manner. The second ordering is also Pt-driven, and represents Pt expelling other Pt atoms to third-nearest neighbour occupancies. Finally, the last ordering is an tetragonal ordering of the Fe and Ni atoms, with Pt atoms unaffected.

The structure of lowest energy for this atomistic model of Fe₄Ni₃Pt is visualised in Fig. 6. It has a clear, uniaxial crystal structure, and consists of alternating layers of Fe and ordered Ni-Pt. The computed MCA of this ordered intermetallic phase is $K_1 = 2.77 \text{ MJm}^{-3}$, approximately three times that of equiatomic FeNi. However, within our modelling framework this ground-state structure only becomes thermodynamically stable at low temperatures, suggesting it will be challenging to synthesise it in the laboratory. This low atomic ordering temperature is associated with an increased configurational entropy contribution for a three-component system over that donated by a binary composition, an aspect which will tend to drive down atomic ordering temperatures. In addition, in our simulations, ordering between Pt and other elements at higher temperature ‘lock’ the Pt atoms to particular lattice sites at relatively high temperatures, limiting the availability of lattice sites that allow Fe and Ni to freely interchange positions and therefore inhibiting atomic ordering.

These results, therefore, present a mixed picture. On one hand, adding Pt to the FeNi base composition clearly has the potential to produce a phase with a ground

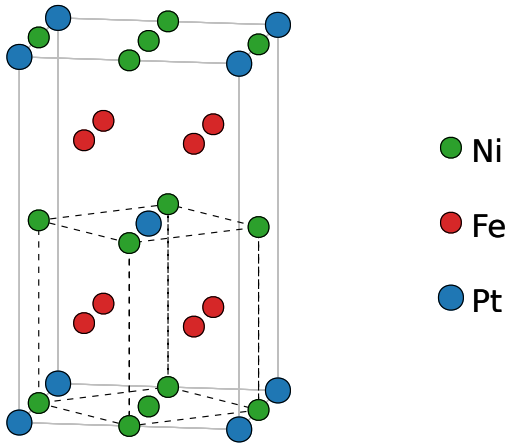


FIG. 6. The predicted ground state of $\text{Fe}_4\text{Ni}_3\text{Pt}$ —a tetragonal, atomically ordered, intermetallic phase. The conventional, cubic unit cell of the underlying fcc lattice is marked with black, dashed lines. The MCA of this ordered phase is predicted to be 2.766 MJm^{-3} , approximately three times that of L1_0 FeNi.

state configuration possessing a high magnetocrystalline anisotropy that is significantly higher than that of binary FeNi. However, the increased configurational entropy and inhibited transformational pathways of the Pt-modified composition mean that this ground state configuration is only stable at low temperatures with concomitant synthesis challenges.

C. $X = \text{Al, Co, Pd, Mo, Cr}$

Building off of the previous example of (FeNi)Pt, to demonstrate the efficacy of our approach for searching for ordered, intermetallic phases with large predicted magnetocrystalline anisotropy energies, and to examine whether alloying provides a viable, cost-effective route for producing atomically ordered L1_0 FeNi in the laboratory, we consider five more alloying additions, added individually to the FeNi lattice: $X = \text{Al, Co, Pd, Mo, Cr}$. Al is chosen as a light abundant element known to form intermetallic phases with both Fe and Ni [69]. Co is chosen as it is known to provide a higher Curie temperature than Fe [26], potentially leading to improved magnetic properties. Pd, with an isoelectronic valence structure to Pt [70], is chosen for comparison with the earlier results. Finally, Cr and Mo are chosen as early transition metals, to examine whether the early 3d transition metals will have an impact on atomic ordering.

Once again, we first calculate an ‘ideal’ MCA, assuming that the elemental addition substitutes only on the Ni sites. Results of this calculation are given in the right-hand column of Table III. Intriguingly, the addition of Co results in a notable *decrease* in MCA compared to that of

binary FeNi. This outcome is associated with the Co on the Ni sublattice making a negative contribution to the total magnetic torque in our calculations. The additives Cr, Al, and Mo look promising, as the addition of any of these elements to the Ni sublattice increases the MCA that is predicted by our calculations. It therefore appears that the addition of these elements alters the electronic structure of the material in such a way as to enhance the predicted MCA. This phenomenon has been noted before in other computational studies, *e.g.* in a study of general Fe-Ni-Al systems [69]. Once again, though, we stress that these calculations represent an idealised picture, and the thermodynamic stability of a given phase must be assessed before drawing conclusions as to its suitability as a gap permanent magnet.

To this end, results of the chemical stability analysis for the system Fe_4Ni_3X , for the considered additions, $X = \text{Al, Co, Pd, Mo, Cr}$, are tabulated in III. The chemical stability analysis is always performed for the system modelled in both its paramagnetic and ferromagnetic states, to assess the degree to which chemical order is coupled to the magnetic state. Where an L1_0 ordering is inferred, indicated by $\mathbf{k}_{\text{ord}} = (0, 0, 1)$, the maximally ordered L1_0 structure that is consistent with this type of ordering is derived, and subsequently its MCA is calculated. Our results for predicted chemical ordering demonstrate that the assumption that the additive will substitute for Ni is flawed; our inferred chemical ordering never leads to a perfect L1_0 -like structure and, therefore, the anisotropy is always reduced compared to that obtained from the ‘ideal’ lattice structure. This result demonstrates that it is crucial to simultaneously examine the phase behaviour of a candidate material and quantify its magnetic properties, to ensure that any proposed intermetallic phase will be thermodynamically stable, and thus realizable.

The computed outcomes provided in Table III are examined one by one. Considering first the results for the addition of Al, we see that, for both the paramagnetic and ferromagnetic cases, the concentration wavevector characterising predicted ordering is not commensurate with a simple ordered structure. This outcome is attributed to competing Ni-Al and Fe-Al interactions. This reasoning is supported by experimental finding: the Ni-Al system has a strong tendency to form an intermetallic phase on the fcc lattice [71], while the Fe-Al system forms on a bcc lattice [72]. In our Monte Carlo simulations, the results of which are visualised in the Supplemental Material [66], the (FeNi)Al system tends to phase segregate into Al-rich and Al-deficient regions. Next considering the results for Cr and Co additions, in both cases an L1_0 ordering is predicted only in the case of the system being in the magnetically ordered state while, in contrast, L1_0 ordering is not predicted for the paramagnetic state. For Mo additions, L1_0 ordering is not predicted in either magnetic state. Finally, the results for Pd additions are comparable with those for the addition of Pt, although the ordering temperatures and the MCA values are notably reduced. The decreased ordering temper-

Composition	Magnetic State	T_{ord} (K)	\mathbf{k}_{ord} ($2\pi/a$)	ΔFe	ΔNi	ΔX	MCA (MJm^{-3})		M (μ_B/atom)	
							Holistic	Ideal	Holistic	Ideal
FeNi	PM	175	(0, 0.675, 0.675)	0.707	-0.707		—		—	
	FM	507	(0, 0, 1)	0.707	-0.707		0.94	0.94	1.66	1.66
$\text{Fe}_4\text{Ni}_3\text{Al}$	PM	686	(0, 0.3, 1)	0.115	0.643	-0.758	—		—	
	FM	765	(0, 0.3, 1)	0.462	0.352	-0.814	—	1.66	—	1.46
$\text{Fe}_4\text{Ni}_3\text{Cr}$	PM	136	(0, 0.6, 0.6)	0.285	-0.805	0.520	—		—	
	FM	853	(0, 0, 1)	0.790	-0.220	-0.570	0.26	1.79	1.09	1.13
$\text{Fe}_4\text{Ni}_3\text{Co}$	PM	151	(0, 0, 0)	0.099	-0.751	0.652	—		—	
	FM	433	(0, 0, 1)	0.749	-0.656	-0.092	0.42	0.31	1.75	1.75
$\text{Fe}_4\text{Ni}_3\text{Mo}$	PM	401	(0.4, 0.5, 0.6)	0.169	0.607	-0.776	—		—	
	FM	607	(0, 0.675, 0.675)	0.344	0.470	-0.814	—	1.37	—	1.26
$\text{Fe}_4\text{Ni}_3\text{Pd}$	PM	361	(0, 0, 1)	0.460	0.354	-0.814	0.17		1.63	
	FM	696	(0, 0, 1)	0.813	-0.338	-0.475	0.20	1.05	1.64	1.66
$\text{Fe}_4\text{Ni}_3\text{Pt}$	PM	794	(0, 0, 1)	0.672	0.065	-0.737	0.96		1.63	
	FM	1163	(0, 0, 1)	0.795	-0.237	-0.558	1.22	3.44	1.63	1.66

TABLE III. Computed atomic ordering temperatures (T_{ord}) and concentration wave modes (k_{ord} , Δc_α) for holistic modelling of the preferred ordering induced by an alloying addition, followed by their consequent predicted magnetisations (M), and magnetocrystalline anisotropy energies. Note that we choose to normalise the chemical fluctuation, writing we choose to normalise the chemical fluctuation, writing $\Delta\alpha = \Delta c_\alpha / \|\Delta c_\alpha\|$.

ature is associated with a reduced difference in atomic radius between chemical species, in turn reducing chemical ordering tendencies. The reduced MCA is associated with a reduced spin-orbit coupling in the system, associated with the smaller mass of the Pd ions compared to Pt ions.

III. DISCUSSION

There are three key conclusions that can be drawn from this study. The first is that, when considering the thermodynamic stability of a candidate hard magnetic phase, it is *crucial* to consider its magnetic state as well. Our results for FeNi suggest that L1_0 ordering is *only* predicted once the parent system has ferromagnetically ordered, suggesting that processing of this phase should take place below its Curie temperature and/or in an applied magnetic field, thereby promoting desired atomic ordering [73]. A similar story holds true when considering alloying additions to this system; different treatments of the magnetic state within our modelling can result in different predicted atomic ordering tendencies.

The second key conclusion is that it is vital to assess the thermodynamic stability of any proposed hard magnetic compound. It will always be possible to imagine metastable crystal structures with extraordinary magnetic properties, but it is only by considering phase equilibria, as is conducted in this study, that a holistic assessment can be made about a candidate material's suitability for applications.

Finally, although these results, and in particular results presented for Pt additives in FeNi, suggest that

some alloying additions may yield increased ordering temperatures and crystal structures with improved magnetocrystalline anisotropy compared to the base FeNi binary, it is not the case that all additives promote L1_0 ordering. It is necessary, therefore, to perform a complete stability analysis of a given specified composition, rather than assume attainment of an L1_0 ordered phase from the outset.

Further work should seek to perform high-throughput searches across a wider range of potential compositions, to search for novel, multi-component alloy phases with desirable magnetic properties. Results of these computational studies can be implemented into experimental activities, to more rapidly realize new types of advanced magnetic materials. We are in the process of adapting our codes for such studies.

IV. METHODS

A. The $S^{(2)}$ theory for multicomponent alloys

Our approach for modelling atomic order in multicomponent alloys uses a Landau-type expansion of the free energy of the system about a homogeneous (disordered) reference state to obtain the two-point correlation function, an ASRO parameter, *ab initio*. The effects of the response of the electronic structure and the rearrangement of charge due to the applied inhomogeneous chemical perturbation are fully included. The theory is the natural multicomponent extension of the $S^{(2)}$ theory developed for binary alloys [74, 75], and it has its ground-

ings in statistical physics and the in seminal papers on concentration waves authored by Khachaturyan [20] and Gyorffy and Stocks [74]. Full details of the theory, its implementation, and extensive discussion can be found in earlier works [10–13].

The approach assumes a fixed, ideal lattice, face-centred cubic (fcc) for the alloys studied in this paper, which represents the averaged atomic positions in the solid solution. A description of the atomic arrangements in a substitutional alloy with this fixed underlying lattice is given by the site occupation numbers, $\{\xi_{i\alpha}\}$, where $\xi_{i\alpha}=1$ if site i is occupied by an atom of species α , and $\xi_{i\alpha}=0$ otherwise. Each lattice site must be constrained to have one (and only one) atom sitting on it, expressed as $\sum_{\alpha} \xi_{i\alpha}=1$ for all lattice sites i . The overall concentration of a chemical species, c_{α} is given by $c_{\alpha} = \frac{1}{N} \sum_i \xi_{i\alpha}$, where N is the total number of lattice sites in the system. A natural choice of atomic long-range order parameter is given by the ensemble average of the site occupancies, $c_{i\alpha} = \langle \xi_{i\alpha} \rangle$, where the $\{c_{i\alpha}\}$ are referred to as the site-wise concentrations. In the atomically disordered limit, corresponding to the solid solution at high temperatures, these occupancies will be spatially homogeneous and take the values of the overall concentration of each chemical species, *i.e.* $\lim_{T \rightarrow \infty} c_{i\alpha} = c_{\alpha}$. Below any atomic disorder-order transition, however, the site occupancies acquire a spatial dependence. These spatially dependent occupancies (or concentrations) can be written as a fluctuation to the concentration distribution of the homogeneous system, $c_{i\alpha} = c_{\alpha} + \Delta c_{i\alpha}$. As the underlying system is lattice-based and possesses translational symmetry, it is natural to write these fluctuations in reciprocal space using a concentration wave formalism, as pioneered by Khachaturyan[20]. In this manner we write

$$c_{i\alpha} = c_{\alpha} + \sum_{\mathbf{k}} e^{i\mathbf{k} \cdot \mathbf{R}_i} \Delta c_{\alpha}(\mathbf{k}) \quad (4)$$

to describe a chemical fluctuation, where \mathbf{R}_i is the lattice vector with corresponding occupancy $c_{i\alpha}$. As an illustrative example, Fig. 2 shows L1₀-type crystallographic order imposed on the fcc lattice for an equiatomic, AB binary system, $c_{\alpha} = (\frac{1}{2}, \frac{1}{2})$. The completely L1₀-ordered structure, represented by alternate layers of atoms of species A and B , is described by $\mathbf{k} = \{(0, 0, 1), (0, 0, -1)\}$, with the (normalised) change in concentration $\Delta c_{\alpha} = \frac{1}{\sqrt{2}}(-1, 1)$. This formalism is extensible to multicomponent alloys.

Correlations between atomic species above any disorder-order transition temperature are quantified by the two-point correlation function, written as

$$\Psi_{i\alpha j\alpha'} = \langle \xi_{i\alpha} \xi_{j\alpha'} \rangle - \langle \xi_{i\alpha} \rangle \langle \xi_{j\alpha'} \rangle, \quad (5)$$

which is an atomic short-range order (ASRO) parameter. This quantity is intrinsically related to the energetic cost of chemical fluctuations [10], as ASRO will be dominated by those chemical fluctuations which are least costly energetically.

To find the energy cost we approximate the free energy, Ω , of an alloy with an inhomogeneous site-wise concentration distribution, $\{c_{i\alpha}\}$, by

$$\Omega^{(1)}[\{c_{i\alpha}\}] = -\frac{1}{\beta} \sum_{i\alpha} c_{i\alpha} \ln c_{i\alpha} - \sum_{i\alpha} \nu_{i\alpha} c_{i\alpha} + \langle \Omega_{\text{el}} \rangle_0[\{c_{i\alpha}\}], \quad (6)$$

where the three terms on the right-hand side of Eq. (2) describe entropic contributions, site-wise chemical potentials, and an average of the electronic contribution to the free energy of the system, respectively. The free energy of the system is then expanded about the homogeneous reference state (*i.e.* the solid solution) in terms of the $\{c_{i\alpha}\}$. This Landau-type series expansion is written

$$\Omega^{(1)}[\{c_{i\alpha}\}] = \Omega^{(1)}[\{c_{\alpha}\}] + \sum_{i\alpha} \left. \frac{\partial \Omega^{(1)}}{\partial c_{i\alpha}} \right|_{\{c_{\alpha}\}} \Delta c_{i\alpha} + \frac{1}{2} \sum_{i\alpha; j\alpha'} \left. \frac{\partial^2 \Omega^{(1)}}{\partial c_{i\alpha} \partial c_{j\alpha'}} \right|_{\{c_{\alpha}\}} \Delta c_{i\alpha} \Delta c_{j\alpha'} + \dots \quad (7)$$

The site-wise chemical potentials present in Eq. 6 serve as Lagrange multipliers in the linear response theory, but their variation is not relevant to the underlying physics so terms involving these derivatives are dropped [10–12]. The symmetry of the solid solution at high temperature—and the requirement that any imposed fluctuation conserves the overall concentrations of each chemical species—ensures that the first-order term vanishes. The change in free energy, $\delta \Omega^{(1)}$ as a result of a fluctuation is therefore written (to second order) as

$$\delta \Omega^{(1)} = \frac{1}{2} \sum_{i\alpha; j\alpha'} \Delta c_{i\alpha} [\beta^{-1} C_{\alpha\alpha'}^{-1} - S_{i\alpha; j\alpha'}^{(2)}] \Delta c_{j\alpha'}, \quad (8)$$

where $C_{\alpha\alpha'}^{-1} = \frac{\delta_{\alpha\alpha'}}{c_{\alpha}}$ is associated with the entropic contributions, and the term $-\frac{\partial^2 \langle \Omega_{\text{el}} \rangle_0}{\partial c_{i\alpha} \partial c_{j\alpha'}} \equiv S_{i\alpha; j\alpha'}^{(2)}$ is the second-order concentration derivative of the average energy of the disordered alloy. The evaluation of this term has been covered in depth in earlier works [10, 11] and for brevity we will omit discussion of it here.

It should be noted that $S_{i\alpha; j\alpha'}^{(2)}$ is evaluated in reciprocal space in our codes, and therefore the change in free energy of Eq. 8 is written accordingly as:

$$\delta \Omega^{(1)} = \frac{1}{2} \sum_{\mathbf{k}} \sum_{\alpha, \alpha'} \Delta c_{\alpha}(\mathbf{k}) [\beta^{-1} C_{\alpha\alpha'}^{-1} - S_{\alpha\alpha'}^{(2)}(\mathbf{k})] \Delta c_{\alpha'}(\mathbf{k}). \quad (9)$$

The matrix in square brackets $[\beta^{-1} C_{\alpha\alpha'}^{-1} - S_{\alpha\alpha'}^{(2)}(\mathbf{k})]$, referred to as the chemical stability matrix, is related to an estimate of the ASRO, $\Psi_{i\alpha; j\alpha'}$. (Eigenvalues of the chemical stability matrices for the compounds considered in this study are visualised in the Supplemental Material [66].) When searching for an disorder-order transition, we start with the high temperature solid solution,

lower the temperature and look for the temperature at which the lowest lying eigenvalue of this matrix passes through zero for any \mathbf{k} -vector in the irreducible Brillouin Zone. When this eigenvalue passes through zero at some temperature T_{ord} and wavevector \mathbf{k}_{ord} , we infer the presence of an disorder-order transition with chemical polarisation Δc_α given by the associated eigenvector. In this fashion we can predict both dominant ASRO and also the temperature at which the solid solution becomes unstable and a crystallographically ordered phase emerges.

B. Pairwise Atomistic Model

To explore the alloy phase space further, we map the concentration derivatives of the internal energy of the alloy, $S_{\alpha\alpha'}^{(2)}(\mathbf{k})$, to a pairwise real-space interaction. This real-space model, referred to as the Bragg-Williams model [46, 47], is lattice-based and has a Hamiltonian of the form

$$H = \frac{1}{2} \sum_{i\alpha;j\alpha'} V_{i\alpha;j\alpha'} \xi_{i\alpha} \xi_{j\alpha'}. \quad (10)$$

The effective pairwise interactions, $V_{i\alpha;j\alpha'}$, are recovered from $S_{\alpha\alpha'}^{(2)}(\mathbf{k})$ by means of an inverse Fourier transform. The mapping from reciprocal-space to real-space and fixing of the gauge degree of freedom on the $V_{i\alpha;j\alpha'}$ is specified in earlier works [10–12]. These interactions are assumed to be isotropic and the sum in Eq. 3 is then taken as a sum over coordination shells, *i.e.* first-nearest neighbours, second-nearest neighbours, etc.

C. Monte Carlo Simulations

To investigate the phase behaviour of these systems with this atomistic model, we perform simulated annealing using the Metropolis Monte-Carlo algorithm with Kawasaki dynamics [48]. These dynamics naturally conserve overall concentrations of each chemical species by permitting only swaps of pairs of atoms.

The algorithm starts by initialising the occupancies of each lattice site randomly, with the only constraint being the overall number of atoms of each chemical species, specified by the overall concentrations. A pair of atomic sites (not necessarily nearest-neighbours) is selected at random, and the change in internal energy ΔH resulting from swapping the site occupancies is calculated. If the change in energy is negative ($\Delta H < 0$) the swap is accepted unconditionally, while if the change is positive ($\Delta H > 0$) the swap is accepted with acceptance probability $e^{-\beta\Delta H}$. To collect the configurational contribution to the specific heat capacity (SHC) of the system, we use the fluctuation-dissipation theorem [76] and the expression

$$C = \frac{1}{k_B T^2} (\langle E^2 \rangle - \langle E \rangle^2). \quad (11)$$

To quantify the emergent ASRO in these simulations, we use the conditional probability of finding one species neighbouring another, writing P_n^{pq} to denote the conditional probability of an atom of type q neighbouring an atom of type p on coordination shell n . In the high-temperature limit, these tend to the value c_q , *i.e.* the overall concentration of species q . Divergence from this homogeneous value is indicative of emergent atomic short- and long-range order.

D. Evaluating magnetocrystalline anisotropy *ab initio*

The magnetocrystalline anisotropy of a system describes the change in energy of the system due to a rotation of the magnetisation direction. For a ferromagnet with magnetisation direction $\hat{\mathbf{n}}$, the MCA can be expressed as

$$K = \sum_{\gamma} K_{\gamma} g_{\gamma}(\hat{\mathbf{n}}), \quad (12)$$

where K_{γ} denote MCA coefficients, and g_{γ} denote spherical harmonics fixing the orientation of $\hat{\mathbf{n}}$ with respect to the crystal axes. These spherical harmonics must respect the symmetry of the underlying crystal structure. It is convenient to represent $\hat{\mathbf{n}}$ in spherical polar coordinates by $\hat{\mathbf{n}} = (\sin \theta \cos \phi, \sin \theta \sin \phi, \cos \theta)$, where θ and ϕ denote polar and azimuthal angles respectively in a coordinate frame specified by the crystal axes.

In a uniaxial ferromagnet, the MCA is well-approximated by

$$K = K_1 \sin^2 \theta \quad (13)$$

and the total energy of the system can be written as

$$\mathcal{E}(\hat{\mathbf{n}}) = \mathcal{E}_{\text{iso}} + K_1 \sin^2 \theta, \quad (14)$$

where \mathcal{E}_{iso} represents the isotropic portion of the energy. The MCA coefficient K_1 can be calculated from derivatives of this energy with respect to magnetisation directions. Given an energy of the form in Eq. 14, we have that

$$\frac{\partial \mathcal{E}}{\partial \theta} = K_1 \sin 2\theta. \quad (15)$$

The magnetocrystalline anisotropy difference between the system magnetised in the $\hat{\mathbf{z}}$ and $\hat{\mathbf{x}}$ directions is the sum,

$$\Delta \mathcal{E} = \mathcal{E}([1, 0, 0]) - \mathcal{E}([0, 0, 1]) = K_1. \quad (16)$$

Evaluation of the derivative, $\frac{\partial \mathcal{E}}{\partial \theta}$ at $\theta = \frac{\pi}{4}$ gives K_1 directly, enabling us to obtain the MCA in a one-shot calculation. Evaluation at other angles enables extraction of coefficients of higher-order anisotropy coefficients, if desired.

Using the MARMOT code [49], which works with a fully relativistic formulation of density functional theory

(DFT), these torques can be evaluated *ab initio*. A discussion of the relevant formulae for the torque in terms of key quantities of multiple scattering theory can be found in Refs. [16] and [36].

E. Computational Details

Throughout, the all-electron HUTSEPOT code [41] is used to generate self-consistent, one electron potentials within the KKR formulation of density functional theory (DFT) [17, 18]. Chemical disorder is described within the coherent potential approximation (CPA) [77, 78], while the magnetic disorder of the paramagnetic state is modelled within the disordered local moment (DLM) picture [42–44]. We perform spin-polarised, scalar-relativistic calculations within the atomic sphere approximation (ASA) [79] with an angular momentum cutoff of $l_{\max} = 3$ for basis set expansions, a $20 \times 20 \times 20$ \mathbf{k} -point mesh for integrals over the Brillouin zone, and a 24 point semi-circular Gauss-Legendre grid in the complex plane to integrate over valence energies. We use the local density approximation (LDA) and the exchange-correlation functional is that of Perdew-Wang [80]. The linear response results are obtained from an computational implementation of the theory described in Section IV A and discussed in detail in earlier works [10–12].

Magnetocrystalline anisotropy energies are evaluated using the MARMOT code [49], which takes in HUTSEPOT potentials as a starting point for its evaluation of the magnetic torques described in Section IV D. Rather than include the effects of spin-orbit coupling in an approximate way, by adding another term to the scalar-relativistic Hamiltonian, MARMOT works in a fully relativistic setting in which spin-orbit effects are included naturally. We use parameters consistent with the HUTSEPOT calculations, and other relevant parameters are left at their MARMOT default values. This includes angular sampling of the CPA integral of 240×40 and an adaptive meshing scheme for Brillouin zone integrations.

DATA AVAILABILITY

The data produced for this study are available through Zenodo via the DOI 10.5281/zenodo.10425682. Specific questions should be directed to the corresponding author(s).

CODE AVAILABILITY

The all-electron HUTSEPOT code [41] used for constructing the self-consistent one-electron potentials of DFT is available at hutsepot.jku.at. The code implementing the $S^{(2)}$ theory for multicomponent alloys [10] is available from the authors on reasonable request. The code for performing lattice-based Monte Carlo simulations to study alloy phase behaviour using the obtained atom-atom interchange parameters [11] is available via the DOI 10.5281/zenodo.10379949. The MARMOT code [49], used for evaluating magnetocrystalline anisotropies in this work, is available at warwick.ac.uk/marmotcode.

ACKNOWLEDGMENTS

The authors would like to express their gratitude to Dr Christopher E. Patrick (Department of Materials, University of Oxford) for fruitful discussions, software support, and feedback on the draft version of this manuscript.

This work was supported by the UK Engineering and Physical Sciences Research Council, Grant No. EP/W021331/1, by the U.S. Department of Energy, Office of Basic Energy Sciences under Award Number DE SC0022168 (for atomic insight) and by the U.S. National Science Foundation under Award ID 2118164 (for advanced manufacturing aspects). C.D.W. was also supported by a studentship within the UK Engineering and Physical Sciences Research Council-supported Centre for Doctoral Training in Modelling of Heterogeneous Systems, Grant No. EP/S022848/1.

AUTHOR CONTRIBUTIONS

C.D.W., L.H.L., and J.B.S. conceived the approach. J.B.S. led development of the MARMOT package used for the magnetocrystalline anisotropy calculations and also developed the code for the ASRO linear response calculations. The electronic structure calculations, linear response analysis, and evaluation of magnetocrystalline anisotropy energies were performed by C.D.W. and J.B.S.. Atomistic simulations and subsequent analysis were performed by C.D.W.. The first draft of the manuscript was written by C.D.W. and subsequently input was received from all authors. J.B.S. and L.H.L. supervised the project and led funding acquisition.

COMPETING INTERESTS

The authors declare no competing interests.

-
- [1] M. Sagawa, S. Fujimura, N. Togawa, H. Yamamoto, and Y. Matsuura, *Journal of Applied Physics* **55**, 2083 (1984).
 - [2] J. J. Croat, J. F. Herbst, R. W. Lee, and F. E. Pinkerton, *Journal of Applied Physics* **55**, 2078 (1984).
 - [3] K. Strnat, G. Hoffer, J. Olson, W. Ostertag, and J. J. Becker, *Journal of Applied Physics* **38**, 1001 (1967).
 - [4] L. H. Lewis and F. Jiménez-Villacorta, *Metallurgical and Materials Transactions A* **44**, 2 (2013).
 - [5] R. McCallum, L. Lewis, R. Skomski, M. Kramer, and I. Anderson, *Annual Review of Materials Research* **44**, 451 (2014).
 - [6] K. Smith Stegen, *Energy Policy* **79**, 1 (2015).
 - [7] J. Bai, X. Xu, Y. Duan, G. Zhang, Z. Wang, L. Wang, and C. Zheng, *Scientific Reports* **12**, 6105 (2022).
 - [8] J. Coey, *Scripta Materialia* **67**, 524 (2012).
 - [9] L. H. Lewis, A. Mubarak, E. Poirier, N. Bordeaux, P. Manchanda, A. Kashyap, R. Skomski, J. Goldstein, F. E. Pinkerton, R. K. Mishra, R. C. Kubic Jr, and K. Barmak, *Journal of Physics: Condensed Matter* **26**, 064213 (2014).
 - [10] S. N. Khan, J. B. Staunton, and G. M. Stocks, *Phys. Rev. B* **93**, 054206 (2016).
 - [11] C. D. Woodgate and J. B. Staunton, *Physical Review B* **105**, 115124 (2022).
 - [12] C. D. Woodgate and J. B. Staunton, *Physical Review Materials* **7**, 013801 (2023).
 - [13] C. D. Woodgate, D. Hedlund, L. H. Lewis, and J. B. Staunton, *Physical Review Materials* **7**, 053801 (2023).
 - [14] J. B. Staunton, S. Ostanin, S. S. A. Razee, B. L. Gyorffy, L. Szunyogh, B. Ginatempo, and E. Bruno, *Physical Review Letters* **93**, 257204 (2004).
 - [15] J. B. Staunton, S. Ostanin, S. S. A. Razee, B. Gyorffy, L. Szunyogh, B. Ginatempo, and E. Bruno, *Journal of Physics: Condensed Matter* **16**, S5623 (2004).
 - [16] J. B. Staunton, L. Szunyogh, A. Buruzs, B. L. Gyorffy, S. Ostanin, and L. Udvardi, *Physical Review B* **74**, 144411 (2006).
 - [17] J. S. Faulkner, G. M. Stocks, and Y. Wang, *Multiple scattering theory electronic structure of solids*, 1st ed. (IOP Publishing, Bristol, UK, 2018).
 - [18] R. M. Martin, *Electronic Structure: Basic Theory and Practical Methods* (Cambridge University Press, Cambridge, UK, 2004).
 - [19] P. Soven, *Physical Review* **156**, 809 (1967).
 - [20] A. G. Khachatryan, *Progress in Materials Science* **22**, 1 (1978).
 - [21] R. Skomski and J. Coey, *Scripta Materialia* **112**, 3 (2016).
 - [22] S. Blundell, *Magnetism in condensed matter*, reprint ed., Oxford master series in condensed matter physics No. 4 (Oxford Univ. Press, Oxford, 2014).
 - [23] J. M. D. Coey, *Magnetism and Magnetic Materials*, 1st ed. (Cambridge University Press, 2001).
 - [24] L. D. Landau, E. M. Lifshitz, and L. P. Pitaevskii, *Electrodynamics of Continuous Media*, 2nd ed., Course of Theoretical Physics No. 8 (Elsevier Butterworth-Heinemann, Amsterdam Heidelberg, 2009).
 - [25] J. Coey, *Engineering* **6**, 119 (2020).
 - [26] C. Kittel, *Introduction to Solid State Physics*, 8th ed. (Wiley, Hoboken, NJ, 2005).
 - [27] C. E. Patrick and J. B. Staunton, *Physical Review Materials* **3**, 101401 (2019).
 - [28] J. Bouaziz, C. E. Patrick, and J. B. Staunton, *Physical Review B* **107**, L020401 (2023).
 - [29] S. Okamoto, N. Kikuchi, O. Kitakami, T. Miyazaki, Y. Shimada, and K. Fukamichi, *Physical Review B* **66**, 024413 (2002).
 - [30] H. Shima, K. Oikawa, A. Fujita, K. Fukamichi, K. Ishida, and A. Sakuma, *Physical Review B* **70**, 224408 (2004).
 - [31] H. Kanazawa, G. Lauhoff, and T. Suzuki, *Journal of Applied Physics* **87**, 6143 (2000).
 - [32] A. Sakuma, *Journal of the Physical Society of Japan* **63**, 3053 (1994).
 - [33] T. Mix, F. Bittner, K.-H. Müller, L. Schultz, and T. Woodcock, *Acta Materialia* **128**, 160 (2017).
 - [34] A. Sakuma, *Journal of the Physical Society of Japan* **63**, 1422 (1994).
 - [35] L. Néel, J. Pauleve, R. Pauthenet, J. Laugier, and D. Dautreppe, *Journal of Applied Physics* **35**, 873 (1964).
 - [36] C. D. Woodgate, C. E. Patrick, L. H. Lewis, and J. B. Staunton, *Journal of Applied Physics* **134**, 163905 (2023).
 - [37] L. H. Lewis, F. E. Pinkerton, N. Bordeaux, A. Mubarak, E. Poirier, J. I. Goldstein, R. Skomski, and K. Barmak, *IEEE Magnetics Letters* **5**, 1 (2014).
 - [38] J. Paulevé, A. Chamberod, K. Krebs, and A. Bourret, *Journal of Applied Physics* **39**, 989 (1968).
 - [39] E. Poirier, F. E. Pinkerton, R. Kubic, R. K. Mishra, N. Bordeaux, A. Mubarak, L. H. Lewis, J. I. Goldstein, R. Skomski, and K. Barmak, *Journal of Applied Physics* **117**, 17E318 (2015).
 - [40] A. Montes-Arango, L. Marshall, A. Fortes, N. Bordeaux, S. Langridge, K. Barmak, and L. Lewis, *Acta Materialia* **116**, 263 (2016).
 - [41] M. Hoffmann, A. Ernst, W. Hergert, V. N. Antonov, W. A. Adeagbo, R. M. Geilhufe, and H. Ben Hamed, *Physica Status Solidi (b)* **257**, 1900671 (2020).
 - [42] A. J. Pindor, J. Staunton, G. M. Stocks, and H. Winter, *Journal of Physics F: Metal Physics* **13**, 979 (1983).
 - [43] J. Staunton, B. Gyorffy, A. Pindor, G. Stocks, and H. Winter, *Journal of Magnetism and Magnetic Materials* **45**, 15 (1984).
 - [44] B. L. Gyorffy, A. J. Pindor, J. Staunton, G. M. Stocks, and H. Winter, *Journal of Physics F: Metal Physics* **15**, 1337 (1985).
 - [45] L.-Y. Tian, O. Eriksson, and L. Vitos, *Scientific Reports* **10**, 14766 (2020).
 - [46] W. L. Bragg and E. J. Williams, *Proceedings of the Royal Society of London. Series A, Containing Papers of a Mathematical and Physical Character* **145**, 699 (1934).
 - [47] W. L. Bragg and E. J. Williams, *Proceedings of the Royal Society of London. Series A - Mathematical and Physical Sciences* **151**, 540 (1935).
 - [48] D. P. Landau and K. Binder, *A Guide to Monte Carlo Simulations in Statistical Physics*, 4th ed. (Cambridge University Press, Cambridge, UK, 2014).
 - [49] C. E. Patrick and J. B. Staunton, *Electronic Structure* **4**, 017001 (2022).
 - [50] T. Shima, M. Okamura, S. Mitani, and K. Takanashi, *Journal of Magnetism and Magnetic Materials* **310**, 2213 (2007).
 - [51] M. Mizuguchi, T. Kojima, M. Kotsugi, T. Koganezawa, K. Osaka, and K. Takanashi, *Journal of the Magnetics*

- Society of Japan **35**, 370 (2011).
- [52] T. Kojima, M. Mizuguchi, and K. Takanashi, *Journal of Physics: Conference Series* **266**, 012119 (2011).
 - [53] T. Kojima, M. Mizuguchi, T. Koganezawa, K. Osaka, M. Kotsugi, and K. Takanashi, *Japanese Journal of Applied Physics* **51**, 010204 (2012).
 - [54] T. Kojima, M. Ogiwara, M. Mizuguchi, M. Kotsugi, T. Koganezawa, T. Ohtsuki, T.-Y. Tashiro, and K. Takanashi, *Journal of Physics: Condensed Matter* **26**, 064207 (2014).
 - [55] A. Frisk, B. Lindgren, S. D. Pappas, E. Johansson, and G. Andersson, *Journal of Physics: Condensed Matter* **28**, 406002 (2016).
 - [56] A. Frisk, T. P. A. Hase, P. Svedlindh, E. Johansson, and G. Andersson, *Journal of Physics D: Applied Physics* **50**, 085009 (2017).
 - [57] K. Ito, T. Ichimura, M. Hayashida, T. Nishio, S. Goto, H. Kura, R. Sasaki, M. Tsujikawa, M. Shirai, T. Koganezawa, M. Mizuguchi, Y. Shimada, T. J. Konno, H. Yanagihara, and K. Takanashi, *Journal of Alloys and Compounds* **946**, 169450 (2023).
 - [58] A. Izardar and C. Ederer, *Physical Review Materials* **4**, 054418 (2020).
 - [59] M. Si, A. Izardar, and C. Ederer, *Physical Review Research* **4**, 033161 (2022).
 - [60] M. Werwiński and W. Marciniak, *Journal of Physics D: Applied Physics* **50**, 495008 (2017).
 - [61] Y. Miura, S. Ozaki, Y. Kuwahara, M. Tsujikawa, K. Abe, and M. Shirai, *Journal of Physics: Condensed Matter* **25**, 106005 (2013).
 - [62] D. Tuvshin, T. Ochirkhuyag, S. C. Hong, and D. Odkhuu, *AIP Advances* **11**, 015138 (2021).
 - [63] A. Edström, J. Chico, A. Jakobsson, A. Bergman, and J. Ruzs, *Physical Review B* **90**, 014402 (2014).
 - [64] S. Yamashita and A. Sakuma, *Journal of the Physical Society of Japan* **91**, 093703 (2022).
 - [65] S. Yamashita and A. Sakuma, *Physical Review B* **108**, 054411 (2023).
 - [66] See supplemental material at [URL_will_be_inserted_by_publisher](#) for visualisation of chemical stability matrices, atom-atom interchange parameters, and results for additional Monte Carlo simulations for the alloys studied in this work.
 - [67] L.-Y. Tian, O. Gutfleisch, O. Eriksson, and L. Vitos, *Scientific Reports* **11**, 5253 (2021).
 - [68] O. K. Von Goldbeck, in *IRON—Binary Phase Diagrams* (Springer Berlin Heidelberg, Berlin, Heidelberg, 1982) pp. 91–94.
 - [69] V. V. Sokolovskiy, *Physical Review Materials* **6**, 025402 (2022).
 - [70] A. Montes-Arango, N. Bordeaux, J. Liu, K. Barmak, and L. Lewis, *Journal of Alloys and Compounds* **648**, 845 (2015).
 - [71] H. Okamoto, *Journal of Phase Equilibria & Diffusion* **25**, 394 (2004).
 - [72] O. K. Von Goldbeck, in *IRON—Binary Phase Diagrams* (Springer Berlin Heidelberg, Berlin, Heidelberg, 1982) pp. 5–9.
 - [73] L. H. Lewis and P. S. Stamenov, *Advanced Science* , 2302696 (2023).
 - [74] B. L. Gyorffy and G. M. Stocks, *Phys. Rev. Lett.* **50**, 374 (1983).
 - [75] J. B. Staunton, D. D. Johnson, and F. J. Pinski, *Physical Review B* **50**, 1450 (1994).
 - [76] M. P. Allen and D. J. Tildesley, *Computer Simulation of Liquids*, second edition ed. (Oxford University Press, Oxford, United Kingdom, 2017).
 - [77] J. S. Faulkner and G. M. Stocks, *Physical Review B* **21**, 3222 (1980).
 - [78] D. D. Johnson, D. M. Nicholson, F. J. Pinski, B. L. Gyorffy, and G. M. Stocks, *Physical Review B* **41**, 9701 (1990).
 - [79] G. M. Stocks, W. M. Temmerman, and B. L. Gyorffy, *Physical Review Letters* **41**, 339 (1978).
 - [80] J. P. Perdew and Y. Wang, *Physical Review B* **45**, 13244 (1992).